JCTC Journal of Chemical Theory and Computation

Article

pubs.acs.org/JCTC

Electronic Polarization in Organic Crystals: A Comparative Study of Induced Dipoles and Intramolecular Charge Redistribution Schemes

Gabriele D'Avino,*[,†,§] Luca Muccioli,[†] Claudio Zannoni,[†] David Beljonne,[‡] and Zoltán G. Soos[¶]

[†]Department of Industrial Chemistry "Toso Montanari" and INSTM, University of Bologna, Viale del Risorgimento 4, IT-40136 Bologna, Bologna, Italy

[‡]Laboratory for Chemistry of Novel Materials, University of Mons, Place du Parc 20, BE-7000 Mons, and

[¶]Department of Chemistry, Princeton University, Princeton, New Jersey 08544, United States

Supporting Information

ABSTRACT: Static dielectric tensors and charge carrier polarization energies of a wide set of organic molecules of interest for organic electronics application are calculated with two different approaches: intramolecular charge redistribution and induced dipoles (microlectrostatics). Our results show that, while charge redistribution is better suited for calculating the collective response to an external field, both methods reliably describe the effect of a localized charge carrier in the crystal. Advantages and limitations inherent to the different methods are discussed, also in relation to previous theoretical studies. The agreement with available experimental data confers to our results a predictive character where measurements are missing.

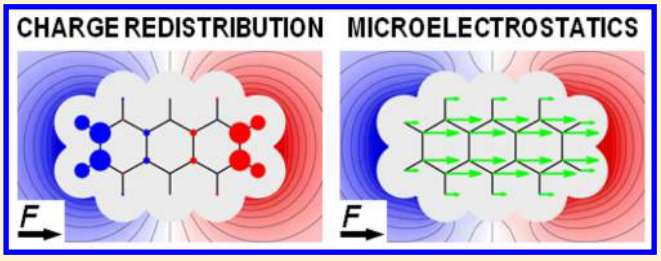

INTRODUCTION

Electrostatics and electronic polarization at the molecular scale govern many fundamental aspects of the functioning of electronic devices based on organic materials. The collective responses to internal or applied electric fields of (macro)-molecular systems, featuring anisotropic charge distributions and polarizabilities, entail nontrivial implications on the energy landscape of charge carriers in bulk materials[1,2] and at their interfaces (level alignment, band bending),[3−6] photoionization measurements,[2,7,8] molecular doping,[8,9] or dielectric screening.[10] The polarization energy (PE) of a localized charge carrier and the dielectric tensor (DT) are key quantities for the above-mentioned properties, and their evaluations with different theoretical methods is the subject of this work.

The conventional picture of organic solids, seen as collections of weakly interacting units preserving their molecular identity, suggests the decoupling of electrostatics and polarization from intermolecular charge transfer, at least to a first approximation.[11] Polarization and electrostatic interactions are in fact 1−2 orders of magnitude stronger than intermolecular charge transfer couplings (electronic bandwidth), and they act on a faster time scale (fs for polarization, instantaneous for electrostatics) than charge dynamics (ps time scale), especially in disordered materials at room temperature.

In the approximation of zero intermolecular overlap, the ground state of a molecular solid is determined by classic electrostatic interactions between quantum objects. Nevertheless, since the electric field experienced by each molecule depends on the polarized charge distribution of all the others, self-consistent intermolecular interactions are responsible for important cooperative effects in molecular solids, i.e. macroscopic responses differing from the sum of those of the individual molecules.[12,13]

Several theoretical approaches have been applied to compute DTs and PEs in organics, differing in the way molecular units and their mutual interactions are described. The simpler family of methods, referred to here as *induced dipole* or *microelectrostatic* (ME) schemes, relies on a classical polarizable points description of electronic polarization, as first proposed by Mott and Littleton for atomic lattices.[14] ME was extended to oligoacene crystals by the seminal work of Munn[15−17] and Silinsh,[18,19] who introduced in a simple but sensible way the information on the molecular structure by distributing the molecular anisotropic polarizability on submolecular units and describing the molecular electrostatic potential via a quadrupole field.[11] The same model, hereafter referred to as original ME, was applied by Verlaak and co-workers to disordered systems, such as grain boundaries in pentacene,[20] organic−organic interfaces,[3] and to a pentacene crystal hosting a molecular dopant.[9] An improved ME scheme, based on a point-charge description of the molecular charge distribution and anisotropic atomic polarizabilities (ME_0 in this work), has been recently applied by some of us to study the energetics of electron−hole separation at different organic heterointerfaces, such as P3HT/PCBM[6] and the interface between two discotic liquid crystals.[21]

Another classic formulation of induced dipole schemes, based on permanent charges and isotropic polarizable points placed at atomic sites, was developed by Applequist[22] and subsequently modified by Thole[23] by introducing a distance-dependent

Received: April 23, 2014
Published: October 8, 2014

   dx.doi.org/10.1021/ct500618w | J. Chem. Theory Comput. 2014, 10, 4959−4971

damping to dipole−dipole interaction, in order to avoid a numerical instability of the model, the so-called dielectric catastrophe.[24] The Applequist-Thole model is nowadays implemented in some common molecular mechanics and dynamics softwares based on polarizable force fields, and several applications to the calculation of polarization energies of charge carriers appeared in the literature.[25−29] Induced dipole schemes were also employed by Brocks and co-workers to evaluate the effect of polarization, and its relation to electronic correlations, in crystals of linear oligoacenes and oligothiophenes.[30]

A more realistic picture of the molecular electronic polarization is obtained in terms of an intramolecular *charge redistribution* (CR) between different regions of a molecule subject to a possibly nonuniform electric field. The concept of distributed nonlocal polarizabilities, i.e. the key quantities governing the CR between molecular subunits, was introduced by Stone.[24,31] The arbitrariness in the choice of subunits was then surpassed by Tsiper and Soos, by considering the redistribution of charge to occur between individual atoms through INDO/S[32] atom−atom polarizabilities.[10,33] In this model, charge redistribution, accounting for about 80−90% of molecular polarizability, coexists with atomic polarizable points, describing the deformation of atomic orbitals in the electric field and ensuring the total molecular polarizability to match a reference value.

Although they significantly differ from the techniques compared in this work, it is worth mentioning other methods based on the approximation of zero intermolecular overlap, for which a number of applications to the calculation of the charge carrier energy landscape in organic solids and at their interfaces have been reported, such as the Valence-Bond/Hartree−Fock (VB/HF)[6,34−36] and quantum mechanics/molecular mechanics (QM/MM)[4,5,37,38] approaches.

In this paper we present a novel and unifying implementation of CR and ME schemes and their application to the calculation of DTs and PEs for a wide set of molecular crystals. In addition, the use of the same molecular inputs, i.e. polarizability tensor and atomic charges, obtained with density functional theory, allows a direct comparative study of the different approaches.

METHODOLOGY

Charge Redistribution and Microelectrostatic Models.

The CR model by Tsiper and Soos describes the polarization of electronic clouds in terms of intramolecular charge flows and induction of dipoles at atomic sites.[10,33] This model is here reviewed, and two ME schemes are derived as particular cases.

In the CR model, the molecular response to a nonuniform electric field is quantified by a discrete set of variables for each atom i: $\{\rho_i, \boldsymbol{\mu}_i\}$. Here, $\rho_i = q_i - q_i^0$ is the variation of the atomic charge (q_i) from its gas-phase value (q_i^0), and $\boldsymbol{\mu}_i$ is the induced atomic dipole moment. The energy of a molecule in an electric field is then written as a quadratic expression in the distortion from gas-phase solution

$$E = \frac{1}{2}\sum_{ij}\rho_i\Pi_{ij}^{-1}\rho_j + \sum_i q_i V_i + \frac{1}{2}\sum_i \boldsymbol{\mu}_i\tilde{\alpha}_i^{-1}\boldsymbol{\mu}_i - \sum_i \boldsymbol{\mu}_i\cdot\mathbf{F}_i \tag{1}$$

where V_i and $\mathbf{F}_i$ are the electric potential and field at atom i, while the tensors Π_{ij}^{-1} and $\tilde{\alpha}_i^{-1}$ measure the stiffness of the polarization through CR and induced dipoles mechanisms, respectively. Specifically, $\tilde{\alpha}_i$ is the linear polarizability tensor associated with atom i, and the atom−atom polarizability tensor Π_{ij} is the susceptibility of atomic charges to a nonuniform applied potential:

$$\Pi_{ij} = -\left(\frac{\partial q_i}{\partial V_j}\right)_0 \tag{2}$$

The Π_{ij} matrix is symmetric and obeys the zero-sum rule $\sum_i\Pi_{ij} = 0$, which ensures the conservation of molecular charge.

The molecular polarization state $\{\rho_i, \boldsymbol{\mu}_i\}$ for a given generalized force $\{V_i, \mathbf{F}_i\}$ then reads

$$\rho_i = -\sum_j \Pi_{ij}V_j \tag{3}$$

$$\mu_i = \tilde{\alpha}_i\mathbf{F}_i \tag{4}$$

In a condensed medium, each atom experiences a possible external applied field, plus the microscopic fields exerted by charges and dipoles on surrounding molecules

$$V_{mi} = V_{mi}^0 + \frac{1}{4\pi\varepsilon_0}\sum_n^{n\neq m}\sum_j\left(\frac{q_{nj}}{R_{mi}^{nj}} + \frac{\boldsymbol{\mu}_{nj}\cdot\mathbf{R}_{mi}^{nj}}{(R_{mi}^{nj})^3}\right) \tag{5}$$

$$\mathbf{F}_{mi} = \mathbf{F}_{mi}^0 + \frac{1}{4\pi\varepsilon_0}\sum_n\sum_j\left(\frac{\delta_{mn}q_{nj}\mathbf{R}_{mi}^{nj}}{(R_{mi}^{nj})^3} + \frac{3g_{mi}^{nj}(\boldsymbol{\mu}_{nj}\cdot\mathbf{R}_{mi}^{nj})\mathbf{R}_{mi}^{nj}}{(R_{mi}^{nj})^5} - \frac{f_{mi}^{nj}\boldsymbol{\mu}_{nj}}{(R_{mi}^{nj})^3}\right) \tag{6}$$

where V_{mi}^0 ($\mathbf{F}_{mi}^0$) is the external potential (field), $\mathbf{R}_{nj}^{mi} = \mathbf{r}_{mi} - \mathbf{r}_{nj}$, the index i (j) runs over the atoms of molecule m (n), and δ_{mn} is the Kronecker delta. g_{mi}^{nj} and f_{mi}^{nj} are functions excluding or damping the interactions between induced dipoles of a given couple of atoms, as discussed later in detail.

The polarization state of N interacting molecules has to be determined self-consistently and the energy of the system can be written as

$$U = \frac{1}{2}\sum_m\sum_i(q_{mi}V_{mi}^{(0)} - \boldsymbol{\mu}_{mi}\cdot\mathbf{F}_{mi}^{(0)}) \tag{7}$$

where $V_{mi}^{(0)}$ and $\mathbf{F}_{mi}^{(0)}$ are the field and potential (cf. eqs 5 and 6) when $\rho_{mi} = 0$ and $\boldsymbol{\mu}_{mi} = 0$. Despite its simplicity, eq 7 includes all the interactions among permanent charges ($q_{mi}^{(0)}$), redistributed charges (ρ_{mi}), and induced dipoles ($\boldsymbol{\mu}_{mi}$), plus the elastic energy involved in molecular polarization (first and third terms on the right-hand side of eq 1).

This general formalism allows the description of mutually interacting polarizable molecules in terms of intramolecular charge redistribution and/or induced dipoles. Hereafter, three particular schemes are derived, differing for the way the molecular polarizability is described. In order to ensure the full comparability of the results, the *same molecular polarizability* tensor is adopted in the different methods, with reference values evaluated at the B3LYP/6-311++G** level, which represents a good comprimise between accuracy and computational cost.[39] We notice that our modeling assumes the polarizability of a molecule in the crystals to be the same as in the vacuum. The agreement between calculated and available experimental data for the DT validates *a posteriori* this assumption, although it is worth mentioning that a theoretical

framework to account for many-body dispersion effects on the polarizability has been recently developed.[40]

The three different schemes considered in this work are the following:

CR: This is a mixed scheme in which the largest contribution to molecular polarizability comes from intramolecular charge flow. The total molecular polarizability, α, is the sum of the contributions from charge redistribution and induced dipoles

$$\alpha^{kl} = \alpha_c^{kl} + \sum_i \tilde{\alpha}_i^{kl} \tag{8}$$

where the indices k and l run over the Cartesian coordinates and

$$\alpha_c^{kl} = \sum_{ij} \Pi_{ij} r_i^k r_j^l \tag{9}$$

is the CR contribution to the polarizability. Π_{ij} matrix elements are evaluated through eq 2 at the INDO/S[32] level of theory, as finite differences of Löwdin atomic charges with respect to an additive potential applied at each atomic site.[10,33] The difference between the reference polarizability tensor and the INDO/S charge-only polarizability, α_c, is distributed over atomic polarizabilities, $\tilde{\alpha}_i$. Induced dipoles, which account for about 10−20% of the total isotropic α, describe the distortion of atomic orbitals in the field, curing some some limitations of the charge flow, such as the lack of out-of-plane polarizability in planar molecules. In this scheme, unscreened interactions between dipoles on different molecules are accounted for, i.e. $g_{mi}^{nj} = f_{mi}^{nj} = 1 - \delta_{mn}$. The difference with the original CR scheme, relevant to PE calculations only, consists of the set of atomic charges $\{q^0\}$ describing the permanent molecular charge distribution, i.e. Löwdin charges in ref 33 and ESP charges[41] in this work.

ME_0: In ME schemes the charge flow among atoms is neglected ($\Pi_{ij} = 0$), and the molecular polarization is described only in terms of induced dipoles. In ME_0 the whole molecular polarizability is distributed over atomic sites and interactions among dipoles on the same molecules are neglected, i.e. $g_{mi}^{nj} = f_{mi}^{nj} = 1 - \delta_{mn}$. This scheme is equivalent to that applied in refs 6 and 21.

ME_a: Also in this case $\Pi_{ij} = 0$, but induced dipoles of atoms on the same molecule are allowed to interact. The divergence of molecular polarizability resulting from too close polarizable points is prevented by damping the interaction between dipoles belonging to the same molecule as in Thole scheme.[23] Specifically, the Tinker-exponential screening functions are here adopted[42]

$$f = 1 - e^{-au^3}$$

$$g = 1 - (1 + au^3)e^{-au^3} \tag{10}$$

where $u = R_{mi}^{nj}(\tilde{\alpha}_i\tilde{\alpha}_j)^{-1/6}$, and a is the screening factor (indices were omitted for simplicity). Unless differently specified, the value $a = 0.125$ is used throughout this paper. By introducing intramolecular dipolar interactions, the actual molecular polarizability differs from the sum of distributed atomic polarizabilities. In this case, we use a set of atomic polarizabilities, $\tilde{\alpha}_i$, such that the molecular finite-field polarizability tensor matches the DFT reference. The drawback of this approach is that the set of $\tilde{\alpha}_i$ has to be determined via a self-consistent iterative procedure for each a value (see the Supporting Information for details).

In all three models, the induced-dipole contribution to molecular polarizability is spread over atoms proportionally to the static atomic polarizability of the corresponding element.[43]

Computational Approach. The self-consistent polarization state of a system of N_a atoms, $\{\rho_i, \boldsymbol{\mu}_i\}$, can be determined by solving a set of $4N_a$ scalar linear equations (eqs 3 and 4 for each atom) with potentials and fields given by eqs 5 and 6. For ME schemes the number of scalar equations reduces to $3N_a$. The solution of the linear systems can be obtained in a few ways, characterized by different stability and computational efficiency.[44,45] Here an iterative scheme is adopted, in which the zero-order approximation of potential ($V_{mi}^{(0)}$) and field ($\mathbf{F}_{mi}^{(0)}$) at atomic sites is obtained for $\{\rho_i = 0, \boldsymbol{\mu}_i = 0\}$ through eqs 5 and 6. $\boldsymbol{\mu}_i$ (and ρ_i in CR) are then updated through eq 4 (3) and used to refine $\mathbf{F}_{mi}$ (V_{mi}). This scheme is iterated up to convergence in the total system energy in eq 7 within a numerical tolerance of 10^{-5} eV, that is typically reached within 30−50 cycles. Induced dipoles and redistributed charges converge to constant values concurrently with the energy of the system.

In the first three iterations, or whenever oscillations in the system energy are detected, the update of $\boldsymbol{\mu}_i$ (and ρ_i) is damped by a factor ω, i.e. $\boldsymbol{\mu}_{mi}^{(k+1)} = \omega\boldsymbol{\mu}_{mi}^{(k)} + (1 - \omega)\tilde{\alpha}_{mi}\mathbf{F}_{mi}^{(k)}$ ($\rho_{mi}^{(k+1)} = \omega\rho_{mi}^{(k)} - (1 - \omega)\sum_j^{j\in m}\Pi_{ij}^m V_{mi}^{(k)}$).[33,45] This expedient prevents divergence of the system energy, while leaving results independent of ω, which should be greater that 0.5 to be effective. This simple numerical strategy, which may be considered as a hybrid between the Jacobi Iterations and the Jacobi Over-Relaxation method, proved to be robust and suitable to our purpouses, although more sophisticate and efficient algorithms for the solution of linear systems related to polarization exist.[44]

Our implementation allowed us to determine the self-consistent polarization state of systems with more than 10000 molecules with serial calculations on an ordinary workstation, with the computation time scaling quadratically with the number of atoms as expected for two-body interactions. Self-consistent ME calculations are 2−4 times faster than CR ones. This is not only due to the smaller number of linear equations to be solved in ME schemes but also to the fact that in CR the evaluation of the fields and potentials generated by point charges has to be performed at every iteration, while in ME this is accomplished only once at the beginning. All the results presented in this work have been obtained with the in-house written Fortran 90 code for MicroElectroStatic Calculations in molecular solids, MESCal.

Systems Studied and Inputs. We considered a selection of organic molecules, which have been subject to fundamental research studies in the context of organic electronics and have found application in different types of devices, such as field effect transistors, solar cells, light emitting diodes, and sensors.

The molecular structure of the chosen compounds is shown in Figure 1. Our set of molecules includes some well-known and characterized hole transporters such as linear oligoacenes (abbreviated as An with n = 2,3,....6, e.g. A6 = hexacene)[46] and linear oligothiophenes with an even number of thiophene rings (Tn with n = 2,4,6, e.g. T4 = quaterthiophene).[47] We consider as well C_{60} Buckminster fullerene, which, together with its derivatives, is one of the most popular electron transporting materials. We complete the selection with other two electron transporters, the dipolar bathophenanthroline (BPH), often used for exciton-blocking layers in organic light emitting diodes,[48] and the very promising perylene bisimide (*N*-bis(2,2,3,3,4,4,4-heptafluorobutyl-1,7-dicyanoperylene-3,4:9,10-

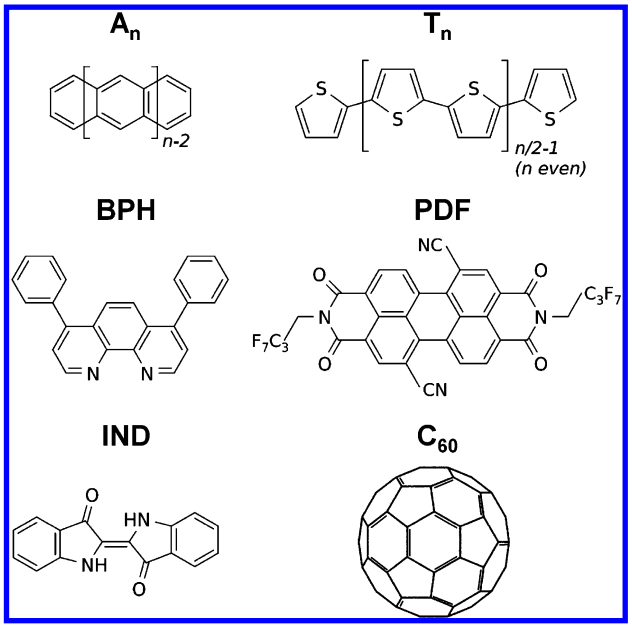

Figure 1. Chemical structures of the molecules considered in this work: linear oligoacenes (A*n*), linear oligothiophenes with an even number of rings (T*n*), bathophenanthroline (BPH), a perylene bisimide derivative with fluorinated chains (PDF), indigo (IND), and fullerene (C_{60}).

bis dicarboximide, PDF),[49] and with an ambipolar semiconducting natural compound, indigo (IND).[50] Common crystal structures for compounds under examinations have been chosen.[51−62]

Polarizability tensors and atomic charges were computed for isolated molecules at the B3LYP/6-311++G** level at the B3LYP/6-31G optimized geometry. Specific calculations have been run for neutral and charged species. DFT and INDO/S charge-only polarizabilities (cf. eq 9) are reported in the Supporting Information. All DFT calculations have been performed with the GAUSSIAN 09[63] suite.

PEs crucially depend on an accurate description of the charge distribution of neutral and charged molecules, which exert strong electric fields in the surrounding space, even in the case of neutral and apolar molecules such as oligoacenes or oligothiophenes.[11,16] As an example, the upper panels of Figure 2 show the electrostatic potential of the A3 molecule in the three planes normal to molecular axes and passing through the molecular centroid. The potential has a quadrupolar character characterized by negative potential regions above and below the molecular plane, which are originated by the π electronic clouds and by hydrogen terminations.

In this work, the molecular electrostatic potential is described in terms of point atomic charges, and in particular we rely on the set of charges derived by fitting the DFT electrostatic potential on the van der Waals surface according to the electrostatic potential fitting scheme (ESP).[41] The reproduction of the molecular dipole moment was also imposed in the fit. In the bottom panels of Figure 2 we show the difference between the DFT potential and that obtained with ESP charges for the A3 molecule. From the figure, we evince that ESP charges provide a careful description of the potential generated by the molecule, also at closest intermolecular distances (approximately twice the van der Waals radius), and reasonably reproduce the quadrupole moment of apolar molecules (see Table S5).

The set of permanent atomic charges does not affect DT calculations, as in the linear response regime their inductive effect is additive to that provided by the external field.

Dielectric Tensor. To obtain the dielectric tensor, we applied a uniform electric field, $\mathbf{F}_0$, along the three Cartesian directions (x, y, z) to spherical molecular clusters of N molecules, obtained by replicating and cutting the experimental crystal structures along their three crystal axis.

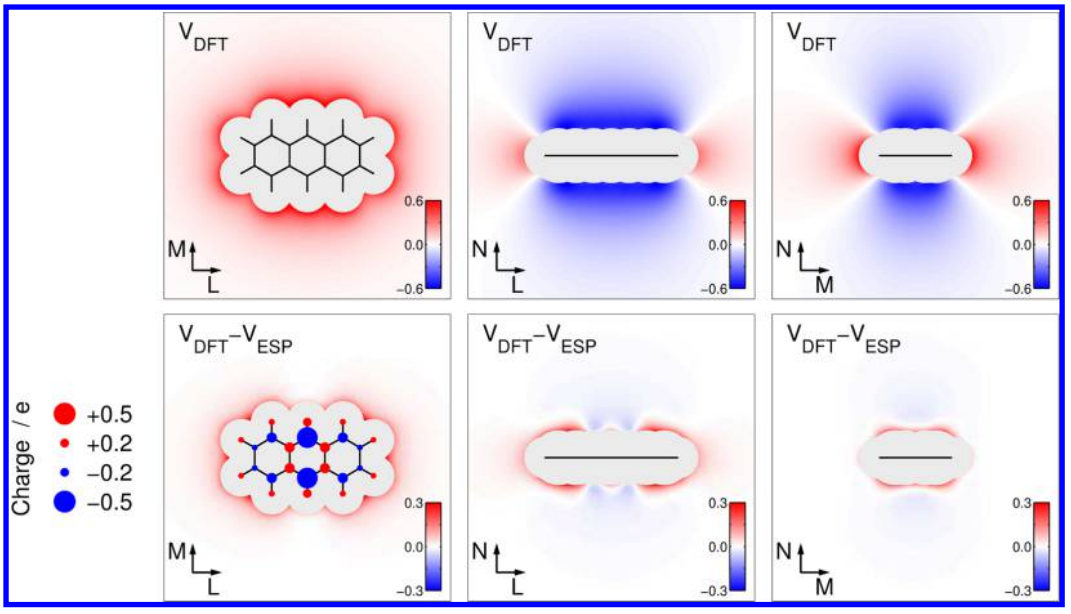

Figure 2. Top: Electrostatic potential of anthracene (A3) in the three planes normal to molecular axes evaluated at the DFT (B3LYP/6-311++G**) level. The color maps highlight the quadrupolar character of A3 charge distribution. Bottom: Difference between the potential calculated with DFT and that generated by ESP atomic charges (shown in the bottom-left panel) obtained at the same level of theory. Potential is expressed in Volts; notice the different color scales in top and bottom panels. The gray area shows the projection of the van der Waals surface in the plane.

dx.doi.org/10.1021/ct500618w | J. Chem. Theory Comput. 2014, 10, 4959−4971

By measuring the induced electric polarization **P** we determine the linear susceptibility tensor of the cluster, ζ_N, according to the equation

$$\mathbf{P} = \varepsilon_0 \zeta_N \mathbf{F}_0 \tag{11}$$

where ε_0 is the vacuum permittivity, and SI units have been used. For large enough clusters, ζ_N scales linearly with the inverse radius, $R^{-1} \propto N^{-1/3}$, and the applied field susceptibility of an infinite sphere ζ is obtained by linear extrapolation, as shown in Figure 3 for A3.

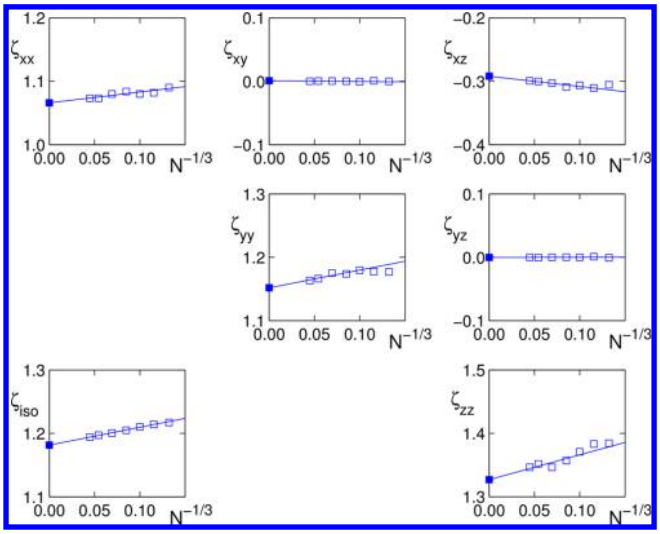

Figure 3. Dielectric susceptibility to a uniform external field (tensor components and isotropic value) of anthracene spherical clusters as a function of the inverse radius (open squares). Linear regressions performed on the results for the five larger clusters (line) are used to extrapolate the values for the infinite crystal (filled squares). Results obtained with CR method.

The relative dielectric tensor κ is instead defined with respect to the total macroscopic field $\mathbf{F}_T$:

$$\mathbf{P} = \varepsilon_0(\kappa - 1)\mathbf{F}_T = \varepsilon_0(\kappa - 1)(\mathbf{F}_0 + \mathbf{F}_d) \tag{12}$$

The total field is the sum of the applied field plus a contribution from the polarized dielectric itself, the so-called depolarization field $\mathbf{F}_d$, which screens the external field inside the material. The dielectric tensor is obtained eliminating $\mathbf{F}_d$ from eq 12, using the textbook depolarization factor for a uniformly polarized dielectric of spherical shape, $\mathbf{F}_d = [-1/(3\varepsilon_0)]\mathbf{P}$:[64]

$$\kappa = \left(1 + \frac{2}{3}\zeta\right)\left(1 - \frac{1}{3}\zeta\right)^{-1} \tag{13}$$

Induced polarization measured on the unit cell at the center of the cluster and on the whole cluster coincide (within 1% for A3), ensuring that edge effects are negligible and the approach reliable. All results shown here are obtained for **P** measured on the central cell. To obtain the bulk DT, one can alternatively apply the depolarization correction to finite-radius spheres and determine their DT and then take the limit for an infinite system. Again, κ values obtained with the two extrapolation procedures are consistent (within 1% for anthracene).

Charge Carrier Polarization Energy. Polarization energies are defined as the difference between crystal and gas phase values of ionization potential and electron affinity:

$$P^+ = IP_{gas} - IP_{cry} \tag{14}$$

$$P^- = EA_{cry} - EA_{gas} \tag{15}$$

PEs measure the contribution from intermolecular interactions in the crystal to hole and electron transport levels and, despite the misleading name, include both an electrostatic and a polarization contribution, plus an additive term due to molecular structural relaxation upon ionization (internal reorganization energy, 0.1−0.3 eV[65,66]). Notice that a different convention for the sign of PE is here adopted with respect to our recent works,[1,6,21] i.e. positive $P^{\pm}$ stabilize the charge carrier in the crystal.

CR and ME allow for the calculation of the electronic component of PE, that is here obtained for spherical clusters of N molecules as

$$P_N^{\pm} = U_N^0 - U_N^{\pm} \tag{16}$$

where U_N^0, U_N^+, and U_N^- are the energies (see eq 7) of the neutral, positively, and negatively charged cluster of N molecules, respectively. In charged systems the ion is placed at the molecule at the center of the cluster. PE scales linearly with R^{-1}, hence results for infinite crystals are obtained by extrapolation as illustrated in Figure 4.

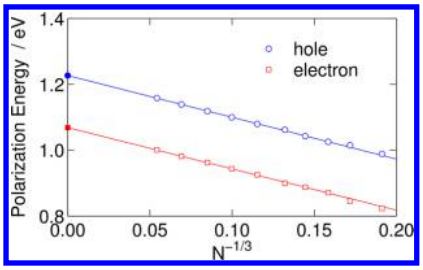

Figure 4. Polarization energy of anthracene for holes (blue circles) and electrons (red squares) as a function of the inverse radius of the spherical cluster. Empty symbols refer to values obtained for finite-size clusters, solid lines are linear regressions, and filled symbols are extrapolated values for the infinite crystal. Results are obtained with the ME_a method.

RESULTS AND DISCUSSION

Molecules in an Electric Field. Before discussing the DT and PE, we present the results of calculations on isolated molecules subject to a uniform electric field. By taking A3 and A6 as examples of modestly and highly polarizable molecules, we analyze the mechanism of molecular polarization in ME and CR, setting the basis for the following discussion.

For such a purpose, we applied a field of magnitude F_0 = 0.0514 V Å^{-1} = 10^{-3} au, along the three molecular axes, and measured the electrostatic potential generated by the polarized molecule in the surrounding space with different methods. We explicitly verified that the applied field induces a linear response in DFT (B3LYP/6-311++G**) calculations, which are here used as a reference. As the DFT linear polarizability is used as input in CR and ME schemes, all calculations yield the same molecular dipole.

The upper panels of Figure 5 show $\delta V = V(F = F_0) - V(F = 0)$ computed at DFT level in the three planes normal to the A3 molecular axes and passing through its centroid. δV can be interpreted as the electrostatic potential generated by the induced charge distribution and is dominated by the induced

dx.doi.org/10.1021/ct500618w | J. Chem. Theory Comput. 2014, 10, 4959−4971

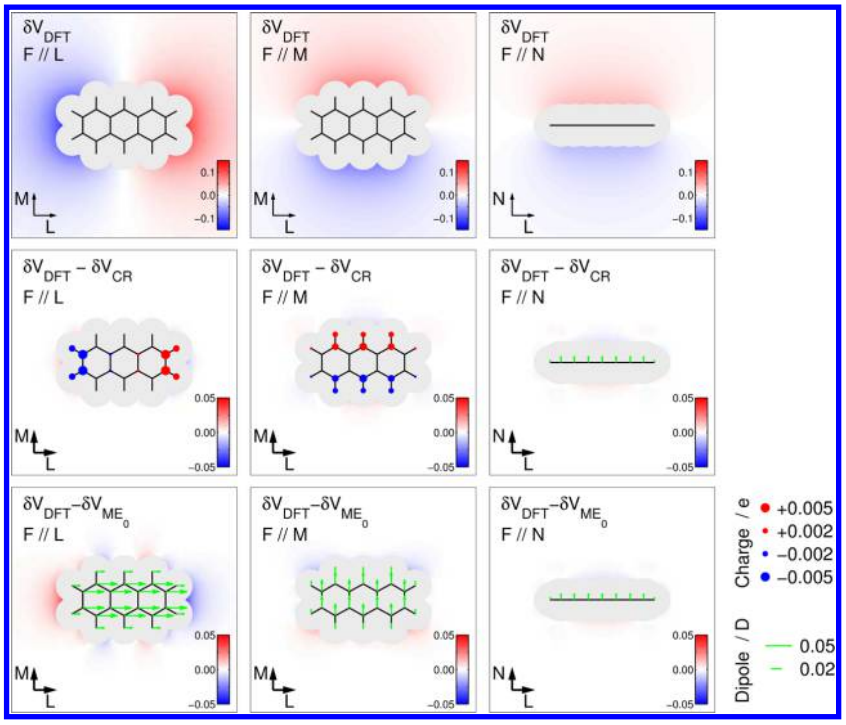

Figure 5. Top: Electrostatic potential generated by the charge distribution induced by a uniform electric field, $\delta V = V(F = F_0) - V(F = 0)$, in the A3 molecule, evaluated at the DFT (B3LYP/6-311++G**) level. The field has a magnitude of 0.0514 V Å^{-1} and direction specified in each panel. Middle/Bottom: Difference between δV evaluated at the DFT and CR/ME$_0$ level. Redistributed charges ρ_i and induced dipoles μ_i are represented in the relevant panels. Potential is expressed in Volts; notice the different color scales in the different panels. The gray area shows the projection of the van der Waals surface in the plane. While CR and DFT results are in close agreement, ME is slightly less accurate when the applied field is parallel to the long molecular axis.

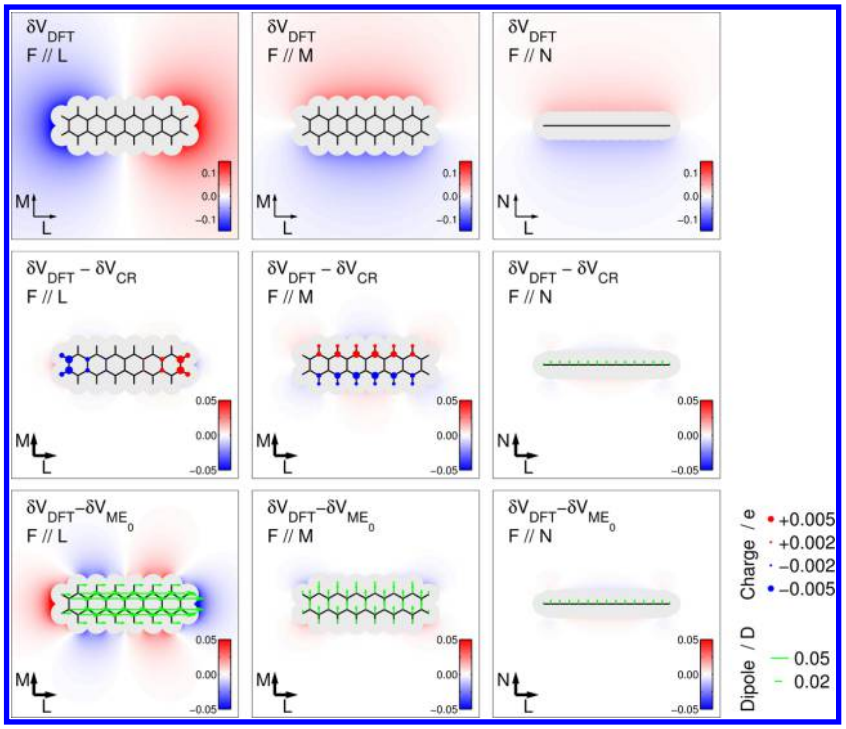

Figure 6. Same as Figure 5 for the A6 molecule. In this case the discrepancy between ME and DFT results when the applied field is parallel to the long molecular axis is much larger than in A3 (Figure 5).

dipole term. The middle (bottom) panels of Figure 5 show instead the difference between the DFT and CR (ME$_0$) values of δV. ME$_a$ results for A3 are similar to ME$_0$ ones and are shown in Figure S1.

It is quite instructive to look at the induced multipoles, i.e. charges and dipoles, which are represented in the relevant panels as circles and arrows, respectively. CR, which approximates very well the DFT potential, provides an intuitive

dx.doi.org/10.1021/ct500618w | J. Chem. Theory Comput. 2014, 10, 4959–4971

and physically sound picture of the mechanism of molecular polarization, characterized by regions of excess or deficiency of charge at the two molecular ends. ME schemes do not reach the same level of accuracy, especially when the field is parallel to the long molecular axis. The difference to DFT potential is however small and limited to the close periphery of the molecule. It is worth noticing that when the field is applied perpendicularly to the molecular plane, ME and CR are equivalent as they both rely on induced dipoles.

The electrostatic potential for the highly polarizable A6 molecule is shown in Figure 6. In this case, CR still provides results in close agreement with DFT calculations, while the accuracy of ME when the field is parallel to the long molecular axis is much lower than for A3. Besides, we noticed that the discrepancy to DFT results of ME schemes is slightly reduced by introducing screened intramolecular dipolar interactions, as prescribed in the ME_a model (see Figure S2).

More generally, the lower accuracy of induced dipoles in highly polarizable molecules highlights a limitation of ME schemes in dealing with π-conjugated electrons: the intramolecular charge redistribution along the long axis, being nonlocal in nature, cannot be described with high accuracy by means of an effective dipole picture, even when the best available molecular polarizability is given as input.

Static Dielectric Tensor. ME and CR calculations grant access to the electronic contribution to the real part of the static DT. In discussing the results, we consider first the series of linear oligoacenes, for which calculated and experimental values of DT are plotted in Figure 7 and reported in Table 1. The principal directions of the DT, superimposed to the crystal unit cell, are shown in Figure 8.

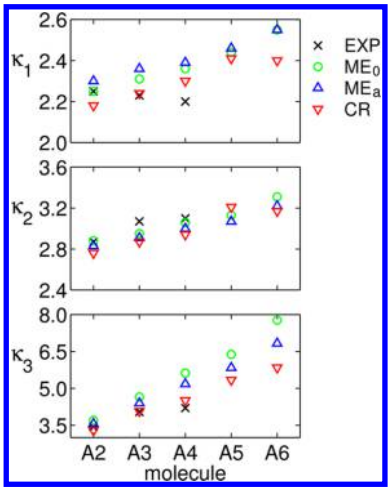

Figure 7. Principal components of the dielectric tensor of linear oligoacenes. For κ_1 and κ_2 a substantial agreement between ME, CR, and experiment is found, while ME_0, and to a lower extent ME_a, overestimates κ_3, especially for highly polarizable molecules.

ME and CR calculations properly reproduce the anisotropy of the DT of A2 and A3 as measured by means of capacitive techniques on single crystals.[67−69] A quantitative agreement with experimental data is obtained for CR, while ME calculations show the tendency to overestimate κ_3 that is parallel to the long molecular axis (see Figure 10), i.e. that of highest polarizability. We notice that the overestimation of κ_3 increases with the long-axis polarizability, and it is partially compensated by introducing the (screened) interaction between induced dipoles on the same molecule, leading to better results for ME_a with respect to ME_0.

Table 1. Calculated and Experimental Dielectric Tensors (Isotropic Values and Principal Components) of Linear Oligoacenes[e]

		κ_{iso}	κ_1	κ_2	κ_3	θ
A2 (3.17)	ME_0[a]	2.95	2.25	2.88	3.70	25.8
	ME_a[a]	2.90	2.30	2.83	3.56	25.5
	CR[a]	2.74	2.18	2.76	3.29	30.0
	EXP[c67]	2.82	2.25	2.87	3.43	28
A3 (3.80)	ME_0[a]	3.31	2.31	2.95	4.65	29.2
	ME_a[a]	3.22	2.36	2.91	4.40	29.2
	CR[a]	3.06	2.24	2.87	4.07	33.0
	CR[b10]	3.06	2.23	2.91	4.03	31.6
	EXP[c68,69]	3.20	2.23	3.07	4.04	28
A4 (4.67)	ME_0[a]	3.68	2.36	3.06	5.62	
	ME_a[a]	3.52	2.39	3.00	5.18	
	CR[a]	3.25	2.30	2.94	4.51	
	EXP[d70]	3.2	2.2	3.1	4.2	
A5 (5.77)	ME_0[a]	3.98	2.44	3.13	6.38	
	ME_a[a]	3.79	2.46	3.07	5.84	
	CR[a]	3.53	2.40	3.10	5.09	
	CR[b45]	3.65	2.41	3.21	5.34	
A6 (7.71)	ME_0[a]	4.54	2.55	3.31	7.77	
	ME_a[a]	4.20	2.55	3.22	6.83	
	CR[a]	3.80	2.40	3.17	5.84	

[a]Present work. [b]Ewald sums. [c]Capacitive measurement (±0.1). [d]Optical measurement: κ_1 and κ_2 correspond to the real part of the refractive index at 2.25 eV, while κ_3 is obtained from a combined fit of ellipsometry and absorption spectra.[70] [e]The Clausius-Mossotti dielectric constants are reported between brackets. In monoclinic crystals (A2, A3) κ_2 is parallel to crystal axis b and θ is the angle between a and κ_1. For monoclinic systems (A4, A5, A6) κ eigenvectors are reported in Table S6.

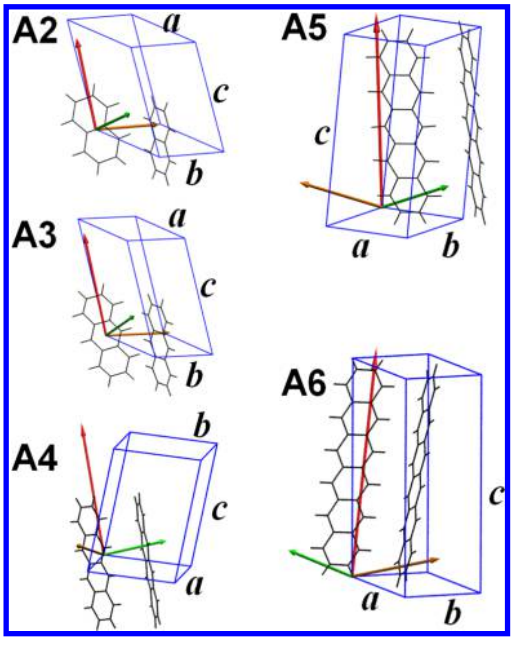

Figure 8. Principal axes of the dielectric tensor of oligoacenes drawn on the crystal unit cell: κ_1 (green arrow), κ_2 (orange), and κ_3 (red). The vector lengths are proportional to the magnitude of the corresponding eigenvalues.

dx.doi.org/10.1021/ct500618w | J. Chem. Theory Comput. 2014, 10, 4959−4971

Also in monoclinic A4, A5, and A6 we obtain a good agreement between the different methods for κ_1 and κ_2 and higher values for κ_3 for ME, with ME_a always performing better than ME_0. Moreover, we notice an increase in the discrepancy between ME and CR values for κ_3 with the molecular length, with the relative difference $(\kappa_3^{ME} - \kappa_3^{CR})/\kappa_3^{CR}$ increasing from 12% to 33% (8% to 17%) for ME_0 (ME_a) when going from A2 to A6 (see Figure 7, bottom panel).

The determination of the DT in triclinic systems is experimentally challenging, and to the best of our knowledge this has been obtained via spectroscopic ellipsometry only recently for A4[70] and A5,[71] although the latter study refers to the Campbell polymorph[72] that has not been considered in this work. The static electronic κ can be inferred from optical measurements as the plateau value in the frequency region below the lowest-energy electronic transitions. The comparison with experimental data for A4 confirms the trend obtained for A2 and A3, with CR being the most accurate method and ME overestimating κ_3.

Table 1 also reports (between brackets) the Clausius-Mossotti dielectric constants, $\kappa_{CM} = [1 + (8\pi\alpha_{iso}/3v)][1 - (4\pi\alpha_{iso}/3v)]^{-1}$, here computed with molecular volume v from experimental crystal structures and DFT isotropic molecular polarizabilities reported in the Supporting Information. The Clausius-Mossotti equation largely overestimates the dielectric constant, especially for the more elongated and anisotropic molecules. This result can be explained by the inappropriateness of the assumptions of isotropic medium and spherical molecular cavity made in the derivation of the well-known equation. It is worth mentioning that an expression for the microscopic field inside an ellipsoidal cavity within an anisotropic dielectric has been derived.[73]

The DTs of linear oligoacenes serve here as a benchmark for the different methods in virtue of the availability of accurate experimental data on single crystals (see Figure 7). The best results are obtained for CR, i.e. a method based on a quantum mechanical description of intramolecular charge flows due nonhomogeneous microscopic fields. We notice that our extrapolated CR results for A3 and A5 are fully consistent with those previously reported and obtained with Ewald sums.[10,45] The induced-dipole picture of ME approaches leads instead to worse results, especially for the κ_3 component in highly polarizable molecules. This failure is related to the intrinsic limitations of induced dipoles in describing the polarization of extended π-conjugated clouds, as discussed in the previous section.

In ME_0 the induced dipoles on the atoms of a given molecule react to microscopic fields independently on each other, resulting in additive response and providing the less accurate results for the DT among the methods here considered. The accuracy of induced-dipole approaches is partly recovered in ME_a by introducing interactions between induced dipoles on the same molecule, that however needs to be screened at short distances to avoid divergent behaviors.[23] Intramolecular dipolar interactions not only introduce correlations between the polarization of different molecular regions but are also a source of additional complications. In fact, these self-interactions lead to a nonadditivity of atomic polarizabilities, which in turn depends on the functional form of the dipole field screening.

In this work we purposefully compare systems with the *same molecular* polarizability, consequently in ME_a the distributed atomic polarizabilities (see Figure S3), and hence the DT (see Figure S4), depend on the screening factor a in eq 10. We do not attempt the determination of an optimal a; we rather rely on a value (a = 0.125) that ensures safe convergence of self-consistent calculations and corresponds to screening distances of ∼5 Å.

The dependence of the DT on the screening factor in ME_a has been investigated for C_{60} and A3, as examples of isotropic and anisotropic molecules (see Figure S4). This analysis showed that by tuning a one can obtain a perfect agreement with the experimental dielectric constant of C_{60}. Things are more complicated in the case of anisotropic molecules, where the simultaneous optimization of the different components of the DT cannot be achieved for the same value of the screening factor. For instance, for a = 0.4 we cure the overestimation of the long-axis component of A3, but this is done at the expenses of the accuracy of the others. Moreover, even the best-compromise a depends on the specific system at hand, limiting the predictive usefulness of ME_a.

CR, ME_a, and experimental DTs for the other molecules considered in this study are reported in Table 2, while Figure 9 shows the tensor principal directions. In general, larger values are obtained for ME_a with respect to CR, confirming the trend observed in oligoacenes. Oligothiophenes feature strongly anisotropic DTs with the largest component aligned to the long molecular axis as for linear oligoacenes. Unfortunately, most of the experimental data on oligoacenes' DT are available only for low-temperature polymorphs (characterized by 4 molecules in the unit cell) and do not permit a direct comparison. We, however, notice that the isotropic dielectric constants reported for the low-temperature polymorphs of T4 (κ = 3.7) and T6 (κ = 4.2) are very close to our estimates.[74,75]

The dielectric constant of C_{60} computed with CR is in accordance with the optical measurement[76] but somehow

Table 2. Calculated and Experimental Dielectric Tensors (Isotropic Values and Principal Components) of T2, T4, T6, C_{60}, BPH, IND, and PDF[e]

		κ_{iso}	κ_1	κ_2	κ_3	θ
T2 (3.46)	ME_a[a]	3.12	2.54	2.90	3.91	44.2
	CR[a]	2.99	2.46	2.84	3.66	36.9
T4 (6.07)	ME_a[a]	3.90	2.47	3.01	6.23	32.9
	CR[a]	3.52	2.39	2.91	5.26	35.4
T6 (13.46)	ME_a[a]	5.07	2.58	3.01	9.62	29.3
	CR[a]	4.36	2.50	3.03	7.57	31.6
C_{60} (3.92)	ME_a[a]	4.87				
	CR[a]	3.96				
	EXP[c76]	4.08				
	EXP[d77]	4.4				
BPH (3.73)	ME_a[a]	3.28	2.98	3.28	3.59	
	CR[a]	2.86	2.62	2.85	3.12	
IND (4.81)	ME_a[a]	3.57	3.08	3.51	4.12	176.0
	CR[a]	3.37	2.90	3.29	3.92	165.2
	EXP[b78]	4.3				
PDF (3.56)	ME_a[a]	3.02	1.95	3.23	3.89	
	CR[a]	2.76	1.82	3.05	3.40	

[a]Present work. [b]Effective value from capacitive measurement. [c]Optical measurement (±0.05). [d]Capacitive measurement (±0.2). [e]The Clausius-Mossotti dielectric constants are reported between brackets. In monoclinic T*n* (IND) θ is the angle between a and κ_1 and the crystal axis b is parallel to κ_2 (κ_3). For BPH (tetragonal) κ_1, κ_2, and κ_3 are directed along c, a, and b, respectively. κ eigenvectors of PDF (triclinic) are reported in Table S6.

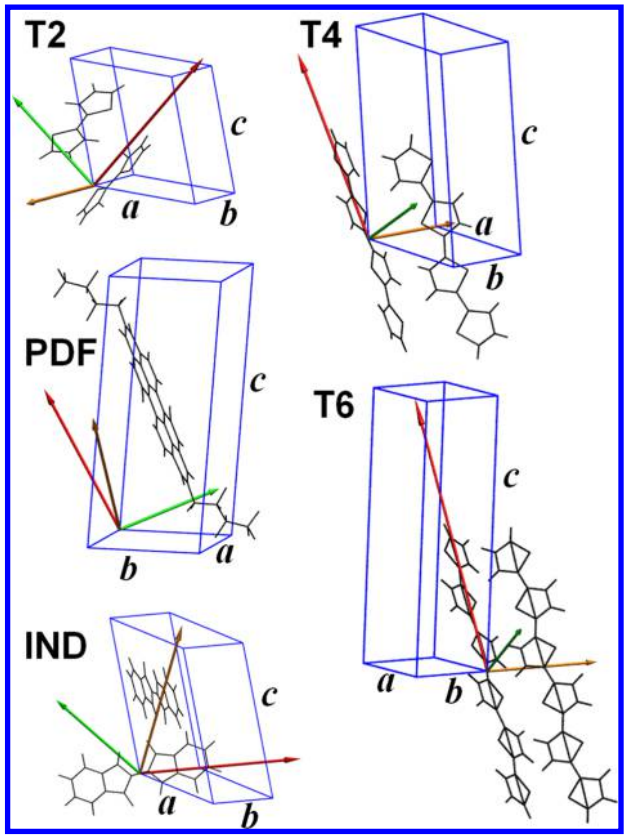

Figure 9. Principal axes of the dielectric tensor of T2, T4, T6, IND, and PDF drawn on the crystal unit cell: κ_1 (green arrow), κ_2 (orange arrow), and κ_3 (red arrow). The vector lengths are proportional to the magnitude of the corresponding eigenvalues.

smaller than the capacitive estimate.[77] Unlike all the other molecules we considered, the Clausius-Mossotti dielectric constant of C_{60}, reported between brackets in Table 1 and Table 2, is in very close agreement with CR calculations and experimental data. This is consistent with the isotropy of the cubic crystal and with the spherical shape of the molecular cavity assumed in the derivation of the Clausius-Mossotti equation. Finally, we notice that both CR and ME_a estimates for IND are significantly smaller that the experimental value, a discrepancy that may be attributed to the intramolecular hydrogen bond characteristic of this molecule, that is not explictly taken into account in our calculations.

Polarization Energy of Charge Carriers. Hole and electron polarization energies of linear oligoacenes, calculated with CR, ME_0, and ME_a, are reported in Table 3 and plotted in Figure 10. Our results show a decreasing trend of PEs with the number of aromatic rings (exception made for ME_0 results reaching a minimum for A5), with larger values for holes than for electrons. Figure 10 and Table 4 also report available experimental data,[19,79] from which we subtracted the specific intramolecular reorganization energies,[65,66] in order to compare the electronic contribution to PE.

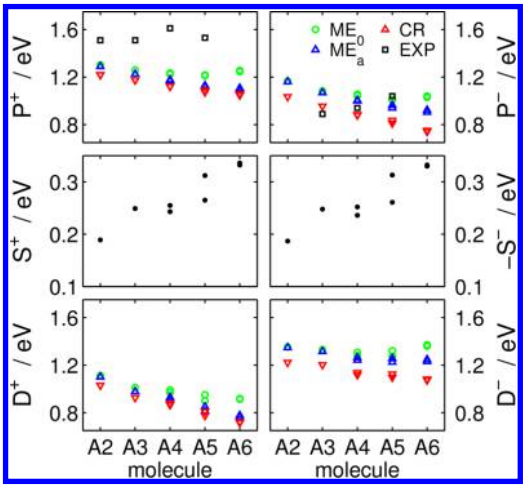

Figure 10. Total, static, and dynamic polarization energies for holes and electrons in linear oligoacenes calculated with CR, ME_0, and ME_a. $S^{\pm}$ values coincide as they depend only on the set of charges and not on the polarization mechanism. For A4, A5, and A6 the two values refer to the nonequivalent molecules in the crystal cell.

The agreement with experiments,[19,79] against which PE calculations have been usually compared, is qualitative and mainly limited to the electron−hole asymmetry, $\Delta P = P^+ - P^- > 0$. Although the origin of this disagreement can be partly due

Table 3. Total, Static, and Dynamic Polarization Energies (in eV) for Holes and Electrons in Acenes, Obtained in This Work with CR, ME_0, and ME_a[a]

		P^+	S^+	D^+	P^-	$-S^-$	D^-
A2	CR	1.22	0.19	1.03	1.03	0.19	1.22
	ME_0	1.30	0.19	1.11	1.17	0.19	1.35
	ME_a	1.29	0.19	1.10	1.16	0.19	1.35
A3	CR	1.18	0.25	0.93	0.95	0.25	1.20
	ME_0	1.26	0.25	1.01	1.08	0.25	1.33
	ME_a	1.23	0.25	0.98	1.07	0.25	1.32
A4	CR	1.12/1.12	0.24/0.26	0.88/0.87	0.88/0.88	0.24/0.25	1.12/1.14
	ME_0	1.23/1.23	0.24/0.26	0.99/0.97	1.04/1.06	0.24/0.25	1.28/1.31
	ME_a	1.18/1.17	0.24/0.26	0.93/0.91	1.00/1.01	0.24/0.25	1.24/1.26
A5	CR	1.07/1.09	0.27/0.31	0.81/0.78	0.84/0.81	0.26/0.31	1.10/1.12
	ME_0	1.22/1.21	0.27/0.31	0.95/0.90	1.01/1.01	0.26/0.31	1.27/1.32
	ME_a	1.12/1.13	0.27/0.31	0.85/0.81	0.96/0.94	0.26/0.31	1.23/1.26
A6	CR	1.05/1.06	0.33/0.34	0.72/0.72	0.75/0.74	0.33/0.33	1.08/1.07
	ME_0	1.25/1.25	0.33/0.34	0.91/0.92	1.04/1.03	0.33/0.33	1.37/1.36
	ME_a	1.09/1.11	0.33/0.34	0.76/0.78	0.92/0.91	0.33/0.33	1.25/1.23

[a]For A4, A5, and A6 the two values refer to the nonequivalent molecules in the crystal cell.

dx.doi.org/10.1021/ct500618w | J. Chem. Theory Comput. 2014, 10, 4959−4971

Table 4. Comparison of Hole and Electron Polarization Energies and Their Difference, $\Delta P = P^+ - P^-$, for A3 and A5[h]

	A3			A5		
	P^+	P^-	ΔP	P^+	P^-	ΔP
CR[a]	1.18	0.95	0.23	1.08	0.82	0.26
ME_a[a]	1.23	1.07	0.16	1.12	0.95	0.17
ME_0[a]	1.26	1.08	0.18	1.21	1.01	0.20
ME[b19]	1.38	1.01	0.37	1.30	0.84	0.46
ME[c20]	1.58	1.06	0.52	1.48	0.89	0.59
CR[d33,45]	1.13	1.07	0.06	1.02	0.99	0.03
CR[e83]	1.38	0.82	0.56			
VB/HF[f34]	0.94	0.73	0.21			
AMOEBA[27]	1.11	0.85	0.26	1.02	0.79	0.23
QM/MM[38]	1.76	1.83	−0.07	1.24	1.49	−0.25
EXP[g19,79]	1.51	0.89	0.62	1.53	1.04	0.49

[a]Present work. [b]Original ME, excess charge distributed at ring centers, quadrupoles from empirical formula. [c]Original ME, excess charge distributed on carbon atoms, quadrupoles as in footnote *b*. [d]CR with permanent charge distribution described by INDO/S Löwdin charges. [e]CR with DFT electron density as permanent charge distribution. [f]Extrapolated from VB/AM1 data in ref 34. [g]See text for discussion on the comparability of calculated and experimental values. [h]Average over the two symmetry nonequivalent molecules.

to the approximations involved in these calculations, we point out that experimental photoelectron spectroscopy data are not the appropriate quantity to assess the accuracy of theoretical estimates. Photoelectron spectroscopy is in fact a surface technique that probes the energy levels of the molecules within a few nanometers from the vacuum interface, while our calculations provide results valid in the bulk limit. Moreover, it is now well established that absolute values of binding energies of electrons in solids are not accessible by photoelectron spectroscopies[80] and that ionization potentials depend on the molecular orientations at the vacuum interface through which the photoelectrons are extracted.[7,81] The quantitative reproduction of photoelectron spectroscopy measurements requires an appropriate modeling of polarization and electrostatic effects in sample morphologies as close as possible to those at which experiments are performed.[8,82] For these reasons, in the following discussion we will mainly focus on methodological aspects of the calculations of PE in the bulk.

Polarization energies are conveniently partitioned in two contributions: $P^{\pm} = S^{\pm} + D^{\pm}$.[34] $S^{\pm}$ is the electrostatic component (or static PE) that is computed as unscreened Coulomb interaction between permanent atomic charges, while $D^{\pm}$ is the contribution coming from the relaxation of molecular polarization (dynamic PE) and is calculated at self-consistency as $P^{\pm} - S^{\pm}$.

Static PEs, shown in the middle panels of Figure 10, depend only on the set of atomic charges. This term has the same physical meaning as the charge-quadrupole interaction of original ME approaches and gives the largest contributions to electron−hole asymmetry, as first recognized by Bounds and Munn.[11,16] $S^{\pm}$ has approximately the same magnitude and opposite sign for holes and electrons, and its absolute value increases with the molecular size, correlating with the magnitude of the quadrupole moment (see Table S5). The values obtained here with ESP charges are consistent with earlier estimates based on different partitioning of excess charge and point quadrupoles over molecular units.[11,16,20] More interestingly, our estimate for $S^{\pm}$ in A3 quantitatively agrees with the one calculated from DFT electron densities.[83] The latter result confirms, as can be also seen from the maps of the electrostatic potential in Figure 2, that ESP atomic charges can achieve approximately the same accuracy in modeling electrostatic interactions as the quantum chemical method employed for their determination. In turn, atomic charges can be easily calculated with standard quantum chemical methods once and for all for each chemical specie and then readily employed in the self-consistent determination of induced multipoles.[6,21]

The dynamic PE, $D^{\pm}$, is a composite term that includes the interaction of induced dipoles (and redistributed charges in CR) with permanent charges and induced multipoles themselves, plus the elastic energy associated with dipoles induction (charge redistribution). While in original ME the charge-induced dipole interaction has the same value for electrons and holes,[11] in our case the adoption of polarizabilities and charges specific to each chemical specie inevitably leads to $D^+ \neq D^-$. For linear oligoacenes we obtain $D^- > D^+$ for the three models considered in this work.

In order to disentangle the different contributions leading to the electron−hole asymmetry in the dynamic PE, $D^+ \neq D^-$, we performed ME and CR calculations by progressively increasing the level of sophistication of our calculation. Figure 11 summarizes the results obtained for A3 (those of other oligoacenes are qualitatively similar), where Roman numbers label the level of calculation.

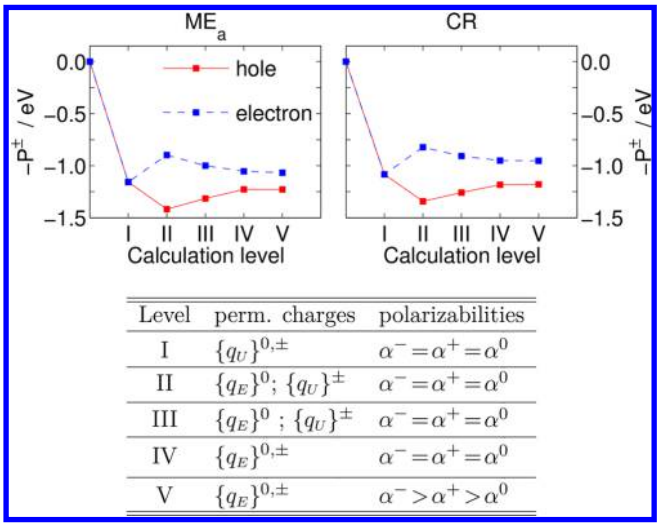

Level	perm. charges	polarizabilities
I	$\{q_U\}^{0,\pm}$	$\alpha^- = \alpha^+ = \alpha^0$
II	$\{q_E\}^0$; $\{q_U\}^{\pm}$	$\alpha^- = \alpha^+ = \alpha^0$
III	$\{q_E\}^0$; $\{q_U\}^{\pm}$	$\alpha^- = \alpha^+ = \alpha^0$
IV	$\{q_E\}^{0,\pm}$	$\alpha^- = \alpha^+ = \alpha^0$
V	$\{q_E\}^{0,\pm}$	$\alpha^- > \alpha^+ > \alpha^0$

Figure 11. Hole and electron polarization energies calculated with CR and ME_a for A3 at different levels of approximation, labeled by roman numbers. The table summarizes the approximations involved at different levels. All PEs are obtained at self-consistency, with the exception of $P_{II}^{\pm} = P_I^{\pm} + S^{\pm}$. $\{q_U\}^Q$ denotes the set of atomic charges obtained by uniformly distributing the molecular charge $Q = 0, \pm 1$ over atoms, $\{q_E\}^Q$ is the set of ESP charges specific to a molecule with net charge Q.

At level I the atomic charges of neutral molecules are set to zero, while the charged molecule bears the same polarizability as neutral ones, and its extra charge is uniformly spread over the atoms. In this case, $P_I^+ = P_I^-$ is equivalent to the charge-induced dipoles interaction of original ME schemes,[11] and its effect is the stabilization of the charge carrier by ∼1.2 eV. In II the electrostatic interaction between the charge carrier and the permanent charge distribution of the surrounding neutral

molecules is introduced as an additive term to $P_I^{\pm}$, leading to the electron−hole asymmetry $P_{II}^{+} - P_{II}^{-} = 2|S^{\pm}|$. This approach to PE calculation (II) is conceptually equivalent to the original ME scheme,[11] though here the electrostatic potential of neutral molecules is described in terms of ESP charges, instead of point quadrupoles. PEs obtained at level II are intrinsically approximate as the polarization and electrostatic contributions are assessed with independent calculations and their additivity is then assumed.

A self-consistent calculation of induced multipoles in the field of permanent charges is presented as III. In this case, the interaction between induced multipoles and the permanent charges of the neutral molecules, not included in calculations I and II, comes into play. This interaction, presenting the same magnitude and opposite sign for holes and electrons, reduces the PE electron−hole asymmetry originated by the electrostatics. The physical interpretation of this effect is straightforward: induced multipoles, by screening the monopole field of the charge carrier, reduce its interaction with the charge distributions of surrounding neutral molecules.

The introduction of atomic ESP charges specific to A3 molecular ions in IV brings a further reduction of ΔP. This effect is mostly due to electronic polarization, which is sensitive to the different extent of localization of the excess charge in the anion and in the cation. The effective radius of the charge distribution of a molecular ion, $r_q = (|\sum_i q_i r_i^2|)^{1/2}$, is 2.2 Å for the electron, 3.3 Å for an uniformly spread excess charge, and 4.2 Å for the hole (r_q depends on the origin of the reference frame, here set to the molecular charge centroid). The trend in r_q is consistent with the larger stabilization provided by the polarizable environment expected for more localized charges. Finally, in V, we introduce the specific polarizabilities of the charged species, whose effect is a small stabilization of the charge carriers energy levels.

A comparison with previous estimates of polarization energies in A3 and A5 is reported in Table 4. Our CR, ME_0, and ME_a results present a close agreement with those recently obtained by Brédas and co-workers[27] with the polarizable force field AMOEBA.[42] This similarity, despite the quite different description of polarization in the CR, ME, and AMOEBA schemes, suggests that the description of polarization energies is largely determined by the quality of microscopic inputs, i.e. permanent multipoles and polarizabilities.

Original ME schemes provide larger electron−hole asymmetries with respect to our calculations (see Table 4), a result due to the missing dielectric screening in computing the charge-quadrupole interaction. However, we cannot rule out a possible role of the inappropriateness of the use of quadrupole field at short distance in those schemes, or inaccuracies in the value of the quadrupole tensor employed, that was obtained with an empirical formula based on both theoretical and experimental data.[11]

CR results in refs 33 and 45 failed to reproduce the electron−hole asymmetry because of the inadequate description of the molecular electrostatic potential provided by INDO/S Löwdin charges. Atomic charges from population analysis are in fact very small for alternant hydrocarbons as oligoacenes (rigorously zero in π-electron theories) and hence not suitable to describe the molecular quadrupole moments. In ref 83, Soos and co-workers proposed a first-order correction to their previous CR results, by computing the interaction between excess charge and induced multipoles with the B3LYP/6-311++G** electron density in a nonself-consistent fashion. Although the two calculations are not fully comparable, the larger value of ΔP obtained for A3 in ref 83 with respect to ours suggests that a fully self-consistent evaluation of induced multipoles in the field of all permament multipoles, as implemented here, is quantitatively important.

Valence bond/Hartree−Fock (VB/HF) calculations for A3 underestimate the values of both P^+ and P^-, as they suffer the poor description of molecular polarizability provided by the semiempirical AM1 Hamiltonian.[34] However, these fully self-consistent calculations confirm that molecular polarization reduces the electron−hole asymmetry originated by electrostatic interactions ($D^- > D^+$). Finally, QM/MM (B3LYP/UFF) results by Norton and Brédas[38] produce larger absolute values of polarization energies with respect to all other approaches and fail qualitatively in describing electron−hole asymmetry.

We now briefly comment on the PEs for the other molecules considered in this work, reported in Table 5, obtained with CR and ME_a. We notice that the two methods provide very similar values for these molecules, with slightly larger PE values in the case of ME_a. Linear oligothiophenes with an even number of rings, being planar quadrupolar molecules arranged in a herringbone crystal packing, behave similarly to oligoacenes, with holes more stable than electrons and with PEs decreasing with the molecular length.

Table 5. Total, Static, and Dynamic Polarization Energies (in eV) for Holes and Electrons for the Non-Acene Molecules, Obtained in This Work with CR and ME_a

		P^+	S^+	D^+	P^-	$-S^-$	D^-
T2	CR	1.22	0.26	0.96	1.06	0.28	1.34
	ME_a	1.28	0.26	1.02	1.18	0.28	1.46
T4	CR	1.04	0.36	0.68	0.75	0.37	1.11
	ME_a	1.09	0.36	0.73	0.92	0.37	1.29
T6	CR	0.93	0.49	0.44	0.62	0.50	1.12
	ME_a	1.00	0.49	0.51	0.94	0.50	1.44
C_{60}	CR	0.92	0.00	0.92	0.92	0.00	0.92
	ME_a	1.05	0.00	1.05	1.05	0.00	1.05
BPH	CR	1.01	0.38	0.63	0.83	0.43	1.26
	ME_a	1.26	0.38	0.87	1.12	0.43	1.55
IND	CR	1.18	0.49	0.69	1.09	0.37	1.46
	ME_a	1.40	0.49	0.91	1.23	0.37	1.59
PDF	CR	0.25	−0.96	1.20	1.20	−0.93	0.27
	ME_a	0.33	−0.96	1.28	1.28	−0.93	0.35

PEs for C_{60} are in quantitative agreement with previous estimates by Munn and co-workers.[84] The identical values obtained for holes and electrons is a direct consequence of our choice to uniformly distribute the molecular charge on atoms. Although ESP analysis provides different values of atomic charges, we consider our assumption to be more appropriate, in virtue of the rotational freedom of C_{60} molecules at room temperature.

For BPH, IND, and PDF, tracing back the computed PEs to molecular features and supramolecular packing is not straightforward. We just remark that the electron−hole asymmetry in the case of PDF molecules is much larger than in other systems here considered yet comparable to values reported for perylene-tetracarboxylic dianhydride (PTCDA).[33,83] The sign (and magnitude) of $\Delta P = P^+ - P^- < 0$ in PDF, opposite to that of acenes and thiophenes, is consistent with the (large and) positive component of the molecular quadrupole and with the slipped-cofacial packing.

dx.doi.org/10.1021/ct500618w | J. Chem. Theory Comput. 2014, 10, 4959−4971

CONCLUSIONS

In this work we have presented a novel and unified implementation of induced-dipole or microelectrostatic (ME) schemes, based on distributed local polarizabilities, and the charge redistribution (CR) approach, based on nonlocal polarizabilities. ME and CR have been applied to compute the dielectric tensor and the polarization energy of a representative set of organic molecular crystals interesting for organic electronics applications.

Our results for the dielectric tensor show that CR quantitatively agrees with available experimental data, as previously reported for anthracene and PTCDA.[10] CR calculations have therefore a predictive character when accurate experimental data are missing, as for the majority of the molecules considered in this work. Conversely, a systematic overestimation of the dielectric tensor component corresponding to the long molecular axis has been found in ME and traced back to an intrinsic limitation of induced dipole pictures in describing the polarization mechanism of extended π-conjugated electronic clouds. Intramolecular dipole−dipole interactions may improve the accuracy of ME, although the predictivity of this kind of schemes is limited by the fact that an optimal value of the screening distance has to be determined by comparison with experimental or CR data.

A close agreement between CR and ME results has been found for what concerns charge carrier polarization energies. The better performances of induced dipoles in the calculation of polarization energies can be explained by the fact that the reaction to the radial field of a localized charge depends on all the components of the crystal polarizability and it is not too sensitive to the overestimation of one of them.

As it is well recognized, an accurate description of the electrostatic potential generated by the molecular charge densities turns out to be essential to assess the energy levels of holes and electrons in organic solids. Microscopic electrostatic fields in neutral supramolecular systems can be nowadays computed with first principle methods[7] and then used to evaluate the electrostatic energies of charge carriers or to include polarization effects when coupled to CR[8,83] or ME schemes. Our implementation relies on potential-derived ESP atomic charges for the molecular charge distribution, which represent an ideal compromise between accuracy and practicality, especially when one is interested in evaluating the charge carrier energy landscape in large and disordered supramolecular systems, as those obtained from molecular dynamics simulations.[6,21]

The implementation of CR and ME schemes presented in this work provides therefore a powerful and yet computationally cheap tool for the investigation of the dielectric properties and the charge carrier energy landscape in bulk organic solids and at their interfaces.

ASSOCIATED CONTENT

Supporting Information

Polarizabilities and quadrupole moments of the molecules considered in this study, additional information on the ME_a model and the eigenvectors of the DT of triclinic crystals. This material is available free of charge via the Internet at http://pubs.acs.org.

AUTHOR INFORMATION

Corresponding Author

*E-mail: gabriele.davino@gmail.com.

Present Address

[§]Department of Physics, University of Liège, Allée du 6 Août 17, BE-4000 Liège, Belgium.

Notes

The authors declare no competing financial interest.

ACKNOWLEDGMENTS

This work was supported by the European Commission Seventh Framework Programme (FP7/2007-2013) under the project MINOTOR, Grant Agreement 228424. G.D. is currently supported by a FP7 Marie Curie BEIPD-COFUND Fellowship. G.D. and L.M. thank M. Lamarra and A. Mityashin for very stimulating discussions. G.D. thanks B. Topham for code sharing and S. Tavazzi and D. Andrienko for useful correspondences.

REFERENCES

(1) Cornil, J.; Verlaak, S.; Martinelli, N.; Mityashin, A.; Olivier, Y.; Van Regemorter, T.; D'Avino, G.; Muccioli, L.; Zannoni, C.; Castet, F.; Beljonne, D.; Heremans, P. *Acc. Chem. Res.* **2013**, *46*, 434−443.

(2) Heimel, G.; Salzmann, I.; Duhm, S.; Koch, N. *Chem. Mater.* **2011**, *23*, 359−377.

(3) Verlaak, S.; Beljonne, D.; Cheyns, D.; Rolin, C.; Linares, M.; Castet, F.; Cornil, J.; Heremans, P. *Adv. Funct. Mater.* **2009**, *19*, 3809−3814.

(4) Yost, S. R.; Wang, L.-P.; Van Voorhis, T. *J. Chem. Phys. C* **2011**, *115*, 14431−14436.

(5) Yost, S. R.; Van Voorhis, T. *J. Phys. Chem. C* **2013**, *117*, 5617−5625.

(6) D'Avino, G.; Mothy, S.; Muccioli, L.; Zannoni, C.; Wang, L.; Cornil, J.; Beljonne, D.; Castet, F. *J. Phys. Chem. C* **2013**, *117*, 12981−12990.

(7) Duhm, S.; Heimel, G.; Salzmann, I.; Glowatzki, H.; Johnson, R. L.; Vollmer, A.; Rabe, J. P.; Koch, N. *Nat. Mater.* **2008**, *7*, 326.

(8) Topham, B. J.; Soos, Z. G. *Phys. Rev. B* **2011**, *84*, 165405.

(9) Mityashin, A.; Olivier, Y.; Van Regemorter, T.; Rolin, C.; Verlaak, S.; Martinelli, N. G.; Beljonne, D.; Cornil, J.; Genoe, J.; Heremans, P. *Adv. Mater.* **2012**, *24*, 1535−1539.

(10) Soos, Z.; Tsiper, E. V.; Pascal, R. *Chem. Phys. Lett.* **2001**, *342*, 652−658.

(11) Silinsh, E. A.; Čápek, V. *Organic Molecular Crystals: Interaction, Localization, and Transport Phenomena*; American Institute of Physics: 1994.

(12) D'Avino, G.; Grisanti, L.; Guasch, J.; Ratera, I.; Veciana, J.; Painelli, A. *J. Am. Chem. Soc.* **2008**, *130*, 12064−12072.

(13) D'Avino, G.; Grisanti, L.; Painelli, A.; Guasch, J.; Ratera, I.; Veciana, J. *CrystEngComm* **2009**, *11*, 2040−2047.

(14) Mott, N. F.; Littleton, M. J. *Trans. Faraday Soc.* **1938**, *34*, 485−499.

(15) Bounds, P.; Munn, R. *Chem. Phys.* **1979**, *44*, 103−112.

(16) Bounds, P.; Munn, R. *Chem. Phys.* **1981**, *59*, 41−45.

(17) Bounds, P.; Munn, R. *Chem. Phys.* **1981**, *59*, 47−53.

(18) Jurgis, A.; Silinsh, E. A. *Phys. Status Solidi B* **1972**, *53*, 735−743.

(19) Sato, N.; Inokuchi, H.; Silinsh, E. A. *Chem. Phys.* **1987**, *115*, 269−277.

(20) Verlaak, S.; Heremans, P. *Phys. Rev. B* **2007**, *75*, 115127.

(21) Idé, J.; Méreau, R.; Ducasse, L.; Castet, F.; Bock, H.; Olivier, Y.; Cornil, J.; Beljonne, D.; D'Avino, G.; Roscioni, O. M.; Muccioli, L.; Zannoni, C. *J. Am. Chem. Soc.* **2014**, *136*, 2911−2920.

(22) Applequist, J.; Carl, J. R.; Fung, K.-K. *J. Am. Chem. Soc.* **1972**, *94*, 2952−2960.

(23) Thole, B. *Chem. Phys.* **1981**, *59*, 341−350.

(24) Stone, A. J. *The Theory of Intermolecular Forces*; Oxford University Press: Oxford, 1996; Vol. 32. Erratum available from www-stone.ch.cam.ac.uk (accessed Sept 15, 2014).
(25) Schrader, M.; Körner, C.; Elschner, C.; Andrienko, D. *J. Mater. Chem.* **2012**, *22*, 22258−22264.
(26) May, F.; Baumeier, B.; Lennartz, C.; Andrienko, D. *Phys. Rev. Lett.* **2012**, *109*, 136401.
(27) Ryno, S. M.; Lee, S. R.; Sears, J. S.; Risko, C.; Brédas, J.-L. *J. Phys. Chem. C* **2013**, *117*, 13853−13860.
(28) Ryno, S. M.; Risko, C.; Brédas, J.-L. *J. Am. Chem. Soc.* **2014**, *136*, 6421−6427.
(29) Gorczak, N.; Swart, M.; Grozema, F. C. *J. Mater. Chem. C* **2014**, *2*, 3467−3475.
(30) Brocks, G.; van den Brink, J.; Morpurgo, A. F. *Phys. Rev. Lett.* **2004**, *93*, 146405.
(31) Stone, A. *Mol. Phys.* **1985**, *56*, 1065−1082.
(32) Zerner, M. C.; Loew, G. H.; Kirchner, R. F.; Mueller-Westerhoff, U. T. *J. Am. Chem. Soc.* **1980**, *102*, 589−599.
(33) Tsiper, E. V.; Soos, Z. G. *Phys. Rev. B* **2001**, *64*, 195124.
(34) Castet, F.; Aurel, P.; Fritsch, A.; Ducasse, L.; Liotard, D.; Linares, M.; Cornil, J.; Beljonne, D. *Phys. Rev. B* **2008**, *77*, 115210.
(35) Martinelli, N. G.; Ide, J.; Sanchez-Carrera, R. S.; Coropceanu, V.; Bredas, J.-L.; Ducasse, L.; Castet, F.; Cornil, J.; Beljonne, D. *J. Phys. Chem. C* **2010**, *114*, 20678−20685.
(36) Idé, J.; Mereau, R.; Ducasse, L.; Castet, F.; Olivier, Y.; Martinelli, N.; Cornil, J.; Beljonne, D. *J. Phys. Chem. B* **2011**, *115*, 5593−5603.
(37) Difley, S.; Wang, L.-P.; Yeganeh, S.; Yost, S. R.; Voorhis, T. V. *Acc. Chem. Res.* **2010**, *43*, 995−1004.
(38) Norton, J. E.; Brédas, J.-L. *J. Am. Chem. Soc.* **2008**, *130*, 12377−12384.
(39) Hickey, A. L.; Rowley, C. N. *J. Phys. Chem. A* **2014**, *118*, 3678−3687.
(40) Tkatchenko, A.; DiStasio, R. A.; Car, R.; Scheffler, M. *Phys. Rev. Lett.* **2012**, *108*, 236402.
(41) Besler, B. H.; Merz, K. M.; Kollman, P. A. *J. Comput. Chem.* **1990**, *11*, 431−439.
(42) Ren, P.; Ponder, J. W. *J. Phys. Chem. B* **2003**, *107*, 5933−5947.
(43) Lide, D. *CRC Handbook of Chemistry and Physics 2004−2005: A Ready-Reference Book of Chemical and Physical Data*; CRC Handbook of Chemistry and Physics, 85th ed.; CRC Press LLC: 2004.
(44) Lipparini, F.; Lagardère, L.; Stamm, B.; Cancès, E.; Schnieders, M.; Ren, P.; Maday, Y.; Piquemal, J.-P. *J. Chem. Theory Comput.* **2014**, *10*, 1638−1651.
(45) Tsiper, E. V.; Soos, Z. G. *Phys. Rev. B* **2003**, *68*, 085301.
(46) Bendikov, M.; Wudl, F.; Perepichka, D. F. *Chem. Rev.* **2004**, *104*, 4891−4946.
(47) Fichou, D. *J. Mater. Chem.* **2000**, *10*, 571−588.
(48) Chan, M. Y.; Lee, C. S.; Lai, S. L.; Fung, M. K.; Wong, F. L.; Sun, H. Y.; Lau, K. M.; Lee, S. T. *J. Appl. Phys.* **2006**, *100*, 094506.
(49) Molinari, A. S.; Alves, H.; Chen, Z.; Facchetti, A.; Morpurgo, A. F. *J. Am. Chem. Soc.* **2009**, *131*, 2462−2463.
(50) Irimia-Vladu, M.; Glowacki, E. D.; Troshin, P. A.; Schwabegger, G.; Leonat, L.; Susarova, D. K.; Krystal, O.; Ullah, M.; Kanbur, Y.; Bodea, M. A.; Razumov, V. F.; Sitter, H.; Bauer, S.; Sariciftci, N. S. *Adv. Mater.* **2012**, *24*, 321−321.
(51) Brock, C. P.; Dunitz, J. D. *Acta Crystallogr., Sect. B: Struct. Crystallogr. Cryst. Chem.* **1982**, *38*, 2218−2228.
(52) Brock, C. P.; Dunitz, J. D. *Acta Crystallogr., Sect. B: Struct. Sci.* **1990**, *46*, 795−806.
(53) Holmes, D.; Kumaraswamy, S.; Matzger, A. J.; Vollhardt, K. P. C. *Chem.—Eur. J.* **1999**, *5*, 3399−3412.
(54) Siegrist, T.; Kloc, C.; Schön, J. H.; Batlogg, B.; Haddon, R. C.; Berg, S.; Thomas, G. A. *Angew. Chem., Int. Ed.* **2001**, *40*, 1732−1736.
(55) Watanabe, M.; Chang, Y. J.; Liu, S.-W.; Chao, T.-H.; Goto, K.; Islam, M. M.; Yuan, C.-H.; Tao, Y.-T.; Shinmyozu, T.; Chow, T. J. *Nat. Chem.* **2012**, *4*, 574−578.
(56) Chaloner, P. A.; Gunatunga, S. R.; Hitchcock, P. B. *Acta Crystallogr., Sect. C: Cryst. Struct. Commun.* **1994**, *50*, 1941−1942.
(57) Siegrist, T.; Kloc, C.; Laudise, R. A.; Katz, H. E.; Haddon, R. C. *Adv. Mater.* **1998**, *10*, 379−382.
(58) Siegrist, T.; Fleming, R.; Haddon, R.; Laudise, R.; Lovinger, A.; Katz, H.; Bridenbaugh, P.; Davis, D. *J. Mater. Res.* **1995**, *10*, 2170−2173.
(59) Andrè, D.; Dworkin, A.; Szwarc, H.; Cèolin, R.; Agafonov, V.; Fabre, C.; Rassat, A.; Straver, L.; Bernier, P.; Zahab, A. *Mol. Phys.* **1992**, *76*, 1311−1317.
(60) Süsse, P.; Steins, M.; Kupcik, V. *Z. Kristallograph.* **1988**, *184*, 269−273.
(61) Jones, B. A.; Ahrens, M. J.; Yoon, M.-H.; Facchetti, A.; Marks, T. J.; Wasielewski, M. R. *Angew. Chem., Int. Ed.* **2004**, *43*, 6363−6366.
(62) Ceolin, R.; Mariaud, M.; Levillain, P.; Rodier, N. *Acta Crystallogr., Sect. B: Struct. Crystallogr. Cryst. Chem.* **1979**, *35*, 1630−1632.
(63) Frisch, M. J. et al. *Gaussian 09 Revision A.1*; Gaussian Inc.: Wallingford, CT, 2009.
(64) Kittel, C. *Introduction to Solid State Physics*, 6th ed.; John Wiley & Sons, Inc.: New York, 1986.
(65) Coropceanu, V.; Malagoli, M.; da Silva Filho, D. A.; Gruhn, N. E.; Bill, T. G.; Brédas, J. L. *Phys. Rev. Lett.* **2002**, *89*, 275503.
(66) Datta, A.; Mohakud, S.; Pati, S. K. *J. Chem. Phys.* **2007**, *126*, 144710.
(67) Munn, R. W.; Williams, D. F. *J. Chem. Phys.* **1973**, *59*, 1742−1746.
(68) Karl, N.; Rohrbacher, H.; Siebert, D. *Phys. Status Solidi A* **1971**, *4*, 105−109.
(69) Munn, R. W.; Nicholson, J. R.; Schwob, H. P.; Williams, D. F. *J. Chem. Phys.* **1973**, *58*, 3828−3832.
(70) Tavazzi, S.; Raimondo, L.; Silvestri, L.; Spearman, P.; Camposeo, A.; Polo, M.; Pisignano, D. *J. Chem. Phys.* **2008**, *128*, 154709.
(71) Dressel, M.; Gompf, B.; Faltermeier, D.; Tripathi, A. K.; Pflaum, J.; Schubert, M. *Opt. Express* **2008**, *16*, 19770−19778.
(72) Campbell, R. B.; Robertson, J. M.; Trotter, J. *Acta Crystallogr.* **1962**, *15*, 289−290.
(73) Luckhurst, G. R.; Zannoni, C. *Proc. R. Soc. London, Ser. A* **1975**, *343*, 389.
(74) Laicini, M.; Spearman, P.; Tavazzi, S.; Borghesi, A. *Phys. Rev. B* **2005**, *71*, 045212.
(75) Munn, R.; Andrzejak, M.; Petelenz, P.; Esposti, A. D.; Taliani, C. *Chem. Phys. Lett.* **2001**, *336*, 357−363.
(76) Eklund, P.; Rao, A.; Wang, Y.; Zhou, P.; Wang, K.-A.; Holden, J.; Dresselhaus, M.; Dresselhaus, G. *Thin Solid Films* **1995**, *257*, 211−232.
(77) Hebard, A. F.; Haddon, R. C.; Fleming, R. M.; Kortan, A. R. *Appl. Phys. Lett.* **1991**, *59*, 2109−2111.
(78) Głowacki, E. D.; Voss, G.; Leonat, L.; Irimia-Vladu, M.; Bauer, S.; Sariciftci, N. S. *Israel J. Chem.* **2012**, *52*, 540−551.
(79) Sato, N.; Seki, K.; Inokuchi, H. *J. Chem. Soc., Faraday Trans. 2* **1981**, *77*, 1621−1633.
(80) Cahen, D.; Kahn, A. *Adv. Mater.* **2003**, *15*, 271−277.
(81) Salzmann, I.; Duhm, S.; Heimel, G.; Oehzelt, M.; Kniprath, R.; Johnson, R. L.; Rabe, J. P.; Koch, N. *J. Am. Chem. Soc.* **2008**, *130*, 12870−12871 PMID: 18771262.
(82) Topham, B. J.; Kumar, M.; Soos, Z. G. *Chem. Phys. Lett.* **2010**, *493*, 251−254.
(83) Sin, J. M.; Tsiper, E. V.; Soos, Z. G. *Europhys. Lett.* **2002**, *60*, 743.
(84) Eilmes, A.; Munn, R. W.; Trolliet, C. *Adv. Mater. Opt. Electr.* **1996**, *6*, 293−296.